

Electrochemical CO₂ reduction in confined space: Enhanced activity of metal catalysts by graphene overlayer

Zheng-Zhe Lin¹  | Xi Chen¹ | Cong Yin² | Lan Yue³ | Fan-Xin Meng⁴

¹Department of Applied Physics, School of Physics and Optoelectronic Engineering, Xidian University, Xi'an, China

²School of Automation Engineering, University of Electronic Science and Technology of China, Chengdu, China

³School of Materials Science and Engineering, Guizhou Minzu University, Guiyang, China

⁴China Zhenhua Group, Yongguang Electronics Co., Ltd. (State-Owned 873 Factory), Guiyang, China

Correspondence

Zheng-Zhe Lin, Department of Applied Physics, School of Physics and Optoelectronic Engineering, Xidian University, Xi'an 710071, China.
Email: zzlin@xidian.edu.cn

Funding information

Postdoctoral Research Project of Shaanxi Province; Fundamental Research Funds for the Central Universities, Grant/Award Numbers: JB180513, XJS18038; Natural Science Basic Research Plan in Shaanxi Province of China, Grant/Award Number: 2018JQ1034; National Natural Science Foundation of China, Grant/Award Numbers: 11847047, 61504031

Summary

In heterogeneous catalysis, space-confined microenvironment can help to modulate catalytic performance and stabilize reaction intermediates. Recently, two-dimensional (2D) confined catalysis opens a new path for enhancing the performance of catalysts. The restricted space between metal surface and 2D overlayer acts as an ideal environment to promote catalytic reactions. By density functional theory calculations, we reveal the significant effect of graphene overlayer to boost CO₂ reduction reaction (CO₂RR) on metal surfaces. Graphene overlayer exhibits strong influence on COOH* and CHO*, as well as suppression to the side reaction of HCOOH. With higher Fermi level than the molecules, the graphene overlayer injects electrons into the nonbonding orbitals of COOH* and CHO*, resulting in charge redistribution and electrostatic interaction between molecules and graphene. Such effect reduces reaction free energies and onset potentials of crucial reaction steps. Our findings reveal a new way to the design of catalysts for CO₂RR.

KEY WORDS

CO₂ reduction, confined catalysis, graphene

1 | INTRODUCTION

The ever-increasing CO₂ emission has led to global warming and given rise to severe environmental problems. To find possible solutions to this problem, CO₂ reduction reaction (CO₂RR) has gained massive attention.^{1–7} On the basis of electrocatalysis, CO₂ can be converted into CH₄ or other hydrocarbons, which is considered to be a green chemistry approach to deal with CO₂ emissions. However, CO₂RR, which requires the participation of multiple electrons, is endothermic and inefficient. On metal surfaces, onset potential is usually

required to proceed CO₂RR. According to previous studies, large onset potential (-0.5 V or more negative) is needed to reach high reaction rate on a variety of metal surfaces.^{8–10} Furthermore, hydrogen evolution reaction ($2H^+ + 2e \rightarrow H_2$) competes with the CO₂RR and makes it less selective. For decades, several kinds of electrocatalysts for CO₂RR had been examined, and Cu has been found to be the most effective in transition metals.^{11–15} However, on Cu electrode, the onset potential of CO₂RR is on the order of -1 V.¹⁶ Until now, the selectivity of catalysts in CO₂RR remains a challenge. Feasible ways to convert CO₂ are in demand.

Emerging two-dimensional (2D) materials, which are rapidly developed in recent years, exhibit rich new physics. 2D materials have open double-sided surfaces with all atoms subject to surface reactions. Many important advances in the chemistry of 2D materials have made use of the open surfaces.^{17–21} Over the last decade, possible applications of 2D materials in catalysis have been attracting considerable interest.^{22–26} In the field of CO₂RR^{27,28} and water splitting,^{29,30} 2D materials were considered as promising catalysts. 2D materials are characterized by their weak interlayer interaction. Accordingly, new chemistry is suggested to be done under the surfaces of the 2D materials. Under the 2D layers, small molecules may be trapped and reactions will occur underneath. By virtue of the confinement effect of 2D overlayer on metal surface, the barriers of catalytic reactions are greatly reduced.^{31–36} Graphene and hexagonal boron nitride overlayers on transition metal surfaces are able to facilitate reactions involving small molecules,^{31,32} with the interface between graphene and metal surface playing a role of confined “nano reactor.” Graphene overlayer is not uniform but full of cracks. Reactant molecules pass through the cracks and perform reactions underneath graphene.^{31,32} Recently, highly ordered SnO₂ nanoparticles assembled between thin TiO₂ nanosheets were utilized to realize efficient CO₂RR with excellent electrochemical stability.³⁷ Considering the feasible intercalation into the interface between 2D material and solid surface, there should be plenty of room for developing new chemistry for CO₂RR in the confined space under 2D overlayer.

In this paper, density functional theory (DFT) calculations are used to investigate the catalytic performance of graphene-covered metal surfaces (Ag, Au, Cu, Ni, Pd, Pt, and Rh) on electrochemical CO₂RR. The improvement of graphene overlayer on CO₂RR catalytic performance of metal surfaces is revealed via the comparison of calculation results between bare and graphene-covered metal surfaces. By free energy diagram, we demonstrate that the reaction free energies of key intermediate steps of CO₂RR are reduced by the confinement effect of graphene overlayer. Accordingly, the onset potentials for CO₂RR to hydrocarbons are lowered by graphene, as well as suppression to side reaction. To uncover the mechanism of graphene overlayer to promote catalytic performance, charge redistribution between graphene and key intermediate molecules is investigated. We find that the promotion effect of graphene originates from the electron injection from graphene to the nonbonding orbitals of COOH* and CHO*. These findings demonstrate that 2D van der Waals overlayer is effective and stable platform

for enhancing the catalytic performance of transition metals for CO₂RR.

2 | THEORETICAL METHODS

2.1 | DFT calculations

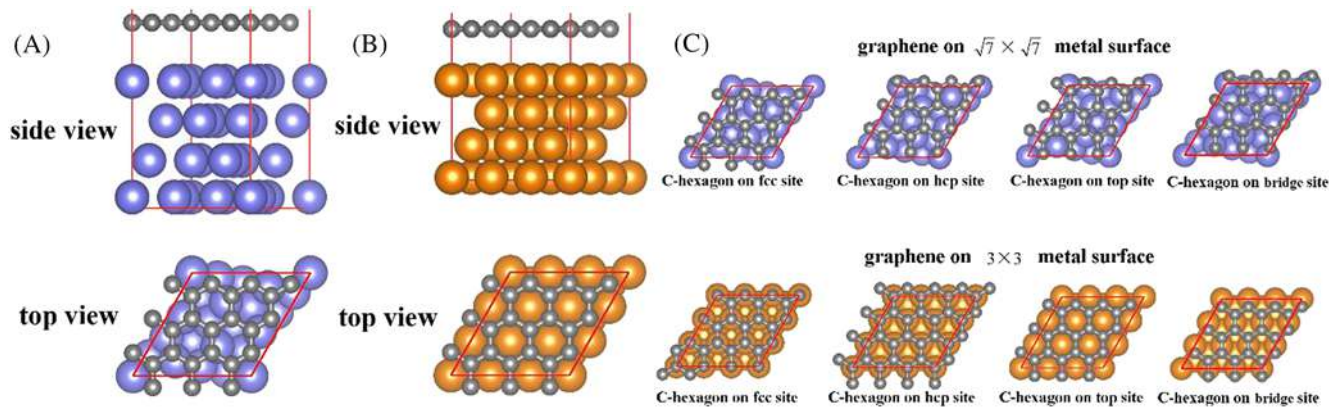
All the spin-polarized DFT calculations are performed using the Vienna Ab initio Simulation Package (VASP).^{38–41} The projector-augmented wave (PAW) pseudopotentials^{42,43} and the generalized gradient approximation for the exchange and correlation of electrons are used. To describe van der Waals interactions, optB88-vdW dispersion-corrected functional,^{44,45} which is reliable for describing dispersive forces in 2D systems,^{46,47} is employed. Plane-wave basis set is used with a kinetic energy cutoff of 400 eV. The Brillouin-zone integration is performed with a $5 \times 5 \times 1$ Monkhorst-Pack grid. The total energy convergence is achieved until total energy difference of successive steps is less than 10^{-5} eV.

2.2 | Simulation model

Repeated slab model is employed to simulate graphene-covered metal surface, in which a graphene layer is covered on metal fcc (111) facet. To minimize lattice mismatch between graphene and metal slabs, lattice constant of 3×3 graphene supercell is adjusted to match that of 3×3 Ni and Cu supercells or $\sqrt{7} \times \sqrt{7}$ Pd, Rh, Pt, Au, and Ag supercells (Scheme 1A,B). The lattice mismatch between graphene and metal substrates is 0.5% to 3.8%. The metal slabs have four atomic layers, with the bottom two layers fixed. Replicas of the system are separated by a vacuum layer of larger than 12 Å. The geometries are relaxed until the Hellmann-Feynman forces are below 0.01 eV/Å. To find the most stable contact geometries of graphene on metal surfaces, we consider different symmetric positions, including C hexagon of graphene above fcc hollow, hcp hollow, atop, and bridge sites (Scheme 1C). By structure relaxation of several different initial configurations, graphene on Cu and Ni (111) surfaces is found to prefer atop site, while on Pd, Rh, Pt, Au, and Ag (111) surfaces is found to prefer fcc hollow site.

2.3 | Free energy

Gibbs free energy calculations are performed according to statistical thermodynamics. With harmonic oscillator approximation, zero-point energies, entropies, and heat capacities are determined by vibrational mode calculations.⁴⁸ At $T = 300$ K, free energies are calculated by



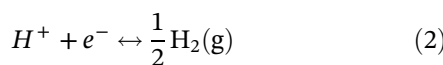
Scheme 1 The configurations of graphene-covered metal surfaces. A, $\sqrt{7} \times \sqrt{7}$ metal supercell for Pd, Rh, Pt, Au, and Ag. B, 3×3 metal supercell for Ni and Cu. The supercell boundary is indicated by red lines. C, Considered possible graphene-metal stacking modes in calculations [Colour figure can be viewed at wileyonlinelibrary.com]

$$G = E_{DFT} + E_{ZPE} + \int_0^T C_p dT - TS, \quad (1)$$

where E_{DFT} is total energy, E_{ZPE} is zero-point energy, $\int_0^T C_p dT$ is integrated heat capacity, and S is entropy. For molecules in gas phase, $\int_0^T C_p dT$ and S are calculated by ideal gas methods.⁴⁸ In above calculations, the fugacity of CO₂ is set 101 325 Pa. The fugacity of H₂O gas is set 3534 Pa, ie, the vapor pressure at 300 K. The aqueous activity of HCOOH is set 0.01, which correspond to a fugacity of 19 Pa.^{15,49}

2.4 | Hydrogen electrode model

Computational hydrogen electrode (CHE) model^{50,51} is employed to evaluate the chemical potential of H⁺ and e⁻. CHE assumes that the chemical potentials of electrodes in equilibrium are measured relative to reversible hydrogen electrode (RHE). In equilibrium, the reaction



is at 0 V. At electrode potential U (relative to RHE), the energy of e⁻ is elevated by $-eU$. The free energy of H⁺ and e⁻ reads

$$G(H^+) + G(e^-) = \frac{1}{2} G(H_2) - eU. \quad (3)$$

Therefore, free energy change of a reaction



is written as

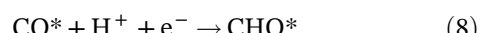
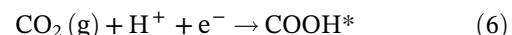
$$\begin{aligned} \Delta G &= G(AH^*) - G(A^*) - G(H^+) - G(e^-) \\ &= G(AH^*) - G(A^*) - \frac{1}{2} G(H_2) + eU. \end{aligned} \quad (5)$$

By Equation (5), the reaction free energy of every elementary step can be evaluated.

3 | RESULTS AND DISCUSSION

3.1 | Reaction mechanism and free energy

Figure 1A shows the reaction process of electrochemical CO₂RR underneath graphene overlayer. On transition metal surface, CO₂ molecules are transformed into hydrocarbons via important intermediates COOH*, CO*, and CHO*. The complete reaction path is shown in Scheme 2. The key steps are



Under different conditions, CO₂RR may result in different hydrocarbons, eg, CH₄ and CH₃OH. For any hydrocarbon production, the COOH* → CO* → CHO* path is the necessary way that must be passed.¹⁶ Figure 1B exhibits a sketch of free energy landscape for these reaction steps. Reactions (6) and (8) are uphill ($\Delta G > 0$), while the free energy in reaction (7) is downhill ($\Delta G < 0$). The free energies of subsequent steps to hydrocarbons are usually downhill or even uphill but with highest free energy below G (COOH*) and G (CHO*). So reactions (6) and (8) are the rate-

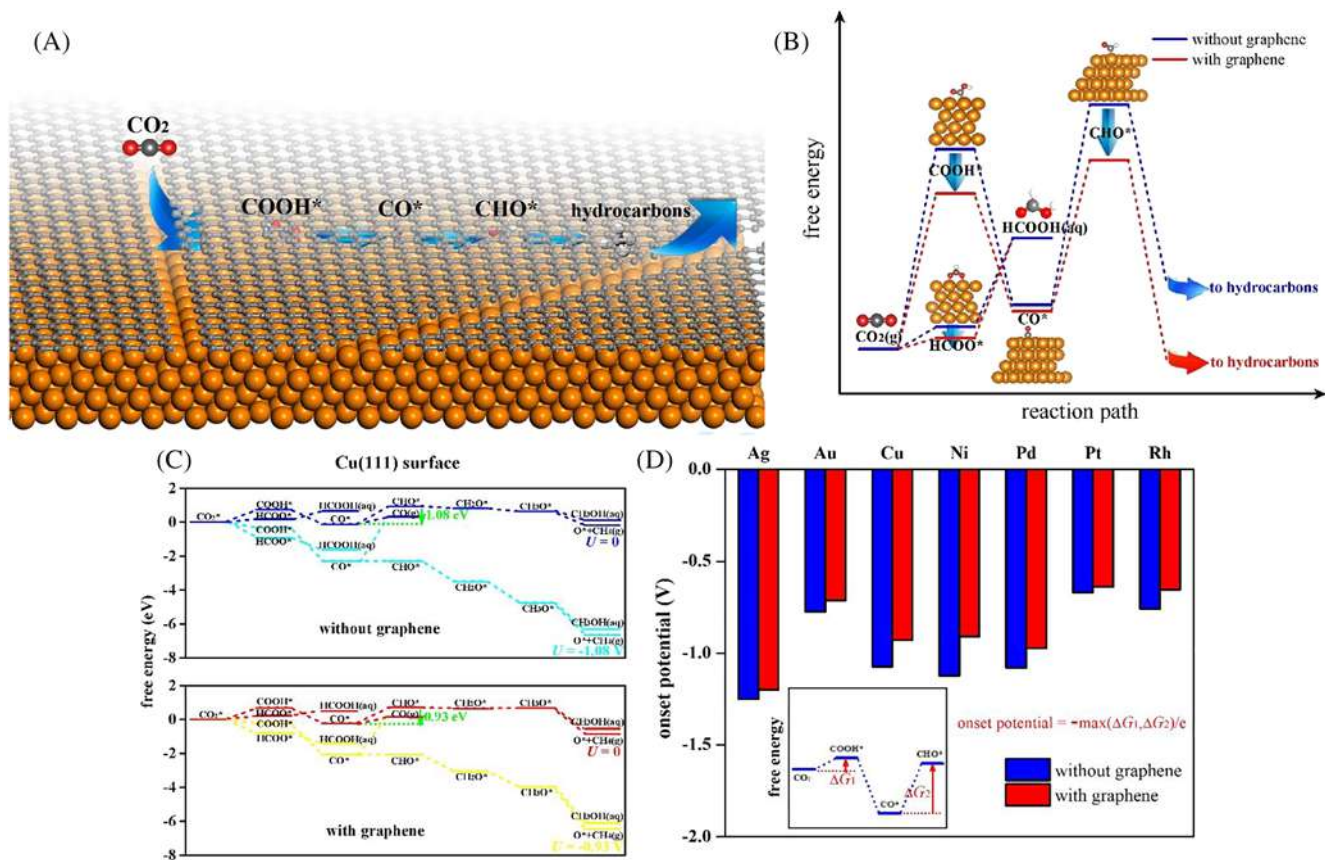
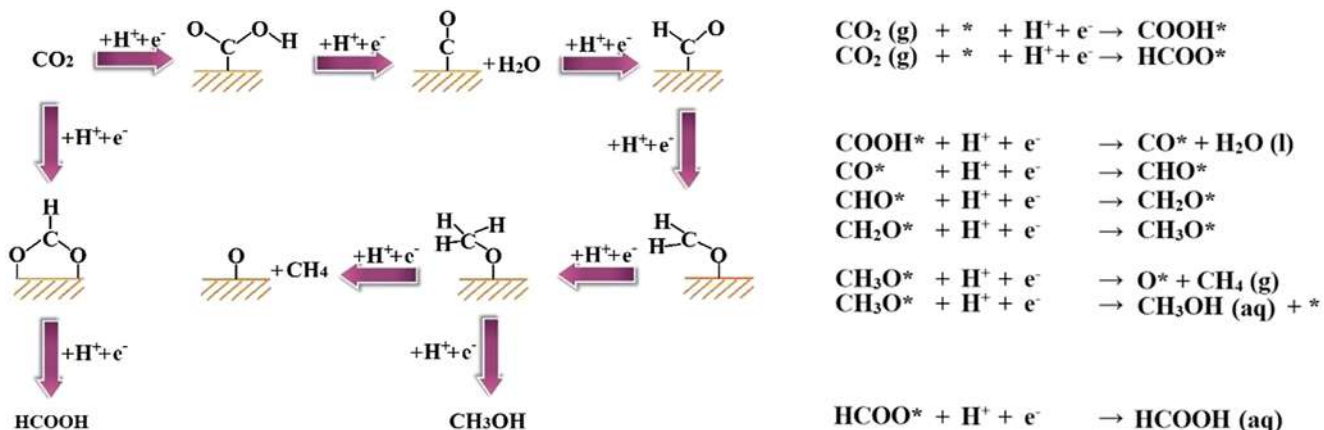


FIGURE 1 The intermediates and free energy of CO₂RR under graphene overlayer. A, A sketch of CO₂RR under graphene. B, A schematic free energy diagram. C, Free energy diagram of CO₂RR on bare Cu (111) surface (at $U = 0$ and -1.08 V) and graphene-covered Cu (111) surface (at $U = 0$ and -0.93 V). D, Onset potentials of CO₂RR on Ag, Au, Cu, Ni, Pd, Pt, and Rh (111) surfaces with/without graphene overlayer [Colour figure can be viewed at wileyonlinelibrary.com]

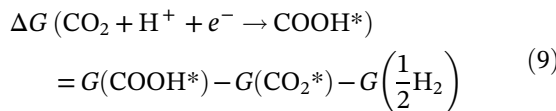


SCHMЕ 2 The reaction path of electrochemical reduction from CO₂ to CH₄ or CH₃OH. The asterisks * in reaction formulas denote transition metal substrate [Colour figure can be viewed at wileyonlinelibrary.com]

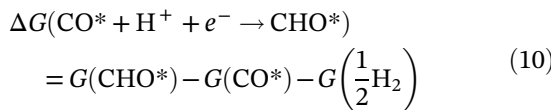
determining steps of the overall CO₂RR process. There also exists a path of side reactions $\text{CO}_2 + \text{H}^+ + \text{e}^- \rightarrow \text{HCOO}^*$ and $\text{HCOO}^* + \text{H}^+ + \text{e}^- \rightarrow \text{HCOOH}$, which leads to HCOOH production. But these two side reactions are all uphill in free energy and thus thermodynamically

unfavorable. In the metal-graphene systems, “catalysis under cover” takes place in the confined space between graphene and metal surface. In the following text, the effect of graphene overlayer on reducing reaction free energy is shown.

To realize the effect of graphene on reactions (6) and (8), we pay attention to the free energy data. For the sake of comparison, let us set the free energies of initial reactants (clean metal substrates and gas-phase molecules) as zero. The detailed data are listed in Table A1 (A2) in Appendix S1 for bare (graphene-covered) metal surfaces. For free energy diagram, see Figure A1 in Appendix S1. Then, the calculated reaction free energies



and



are exhibited in Tables 1 and 2, respectively. Compared with bare metal surfaces, $\Delta G(\text{CO}_2 + \text{H}^+ + e^- \rightarrow \text{COOH}^*)$ and $\Delta G(\text{CO}^* + \text{H}^+ + e^- \rightarrow \text{CHO}^*)$ (shown by arrows in Figure A1 in Appendix S1) on graphene-covered metal surfaces become even lower. It has been reported that molecular adsorption energies and binding strength on metal surfaces are weakened in 2D confined space.^{32,36} Indeed, the confinement effect tends to enhance $G(\text{CO}_2^*)$ (CO_2 adsorbed on metal surface) and $G(\text{COOH}^*)$. But the graphene-molecule interaction may be a factor of lowering $G(\text{COOH}^*)$, and two factors work together. On Ag, Au, and Cu surfaces, the increase of $G(\text{COOH}^*)$ is smaller than the increase of $G(\text{CO}_2^*)$. On graphene-covered Ni, Pd, Pt, and Rh surfaces, $G(\text{COOH}^*)$ are even lower than the values on bare metal

TABLE 1 $\Delta G(\text{CO}_2 + \text{H}^+ + e^- \rightarrow \text{COOH}^*)$ with/without graphene

Substrate	$\Delta G(\text{CO}_2 + \text{H}^+ + e^- \rightarrow \text{COOH}^*)/\text{eV}$		
	without Graphene	with Graphene	Decrease Ratio R
Ag	1.25	1.20	4%
Au	0.77	0.71	8%
Cu	0.75	0.69	8%
Ni	0.11	-0.01	109%
Pd	0.24	0.10	58%
Pt	0.18	-0.04	122%
Rh	0.15	-0.08	153%

The decrease ratio is defined as $R = (\Delta G_{\text{without graphene}} - \Delta G_{\text{with graphene}})/\Delta G_{\text{without graphene}}$.

TABLE 2 $\Delta G(\text{CO}^* + \text{H}^+ + e^- \rightarrow \text{CHO}^*)$ with/without graphene

Substrate	$\Delta G(\text{CO}^* + \text{H}^+ + e^- \rightarrow \text{CHO}^*)/\text{eV}$		
	without Graphene	with Graphene	Decrease Ratio R
Ag	0.53	0.52	2%
Au	0.21	0.17	19%
Cu	1.08	0.93	14%
Ni	1.13	0.91	19%
Pd	1.08	0.97	10%
Pt	0.67	0.64	4%
Rh	0.76	0.66	13%

The decrease ratio is defined as $R = (\Delta G_{\text{without graphene}} - \Delta G_{\text{with graphene}})/\Delta G_{\text{without graphene}}$.

surfaces. Such effect leads to the decrease of $\Delta G(\text{CO}_2 + \text{H}^+ + e^- \rightarrow \text{COOH}^*)$. Similar effect has also been found in Mu et al.³³ The same effect is also found in $\text{CO}^* + \text{H}^+ + e^- \rightarrow \text{CHO}^*$. On graphene-covered Ag and Au surfaces, the increase of $G(\text{CHO}^*)$ is smaller than the increase of $G(\text{CO}^*)$. On graphene-covered Cu, Ni, Pd, Pt, and Rh surfaces, $G(\text{CHO}^*)$ are even lower than the values on bare metal surfaces. On Ni, Pd, Pt, and Rh surfaces, graphene also leads to lower $G(\text{CO}^*)$, but the decrease is not lower than the decrease of $G(\text{CHO}^*)$. In general, the total effect leads to the decrease of $\Delta G(\text{CO}^* + \text{H}^+ + e^- \rightarrow \text{CHO}^*)$.

On bare metal (111) surfaces, $\Delta G(\text{CO}_2 + \text{H}^+ + e^- \rightarrow \text{COOH}^*)$ is in the range of 0.11 to 1.25 eV (Table 1), and $\Delta G(\text{CO}^* + \text{H}^+ + e^- \rightarrow \text{CHO}^*)$ is in the range of 0.21 to 1.13 eV (Table 2). Accordingly, on graphene-covered metal (111) surfaces, $\Delta G(\text{CO}_2 + \text{H}^+ + e^- \rightarrow \text{COOH}^*)$ is in the range of -0.08 to 1.20 eV (Table 1), and $\Delta G(\text{CO}^* + \text{H}^+ + e^- \rightarrow \text{CHO}^*)$ is in the range of 0.17 to 0.97 eV (Table 2). To evaluate the extent of decrease in reaction free energy, we define the decrease ratio

$$R = (\Delta G_{\text{without graphene}} - \Delta G_{\text{with graphene}})/\Delta G_{\text{without graphene}} \quad (11)$$

for both reactions. For $\text{CO}_2 + \text{H}^+ + e^- \rightarrow \text{COOH}^*$, $R(\text{CO}_2 + \text{H}^+ + e^- \rightarrow \text{COOH}^*) = 153\%$ on Rh (111) surfaces is the largest. For $\text{CO}^* + \text{H}^+ + e^- \rightarrow \text{CHO}^*$, $R(\text{CO}^* + \text{H}^+ + e^- \rightarrow \text{CHO}^*) = 19\%$ on Au and Ni (111) surfaces are the largest. It is well known that Cu is a decent electrode in making hydrocarbons. As an example, Figure 1C shows the full free energy landscape on Cu (111) surface with/without graphene overlayer (the free energy of CO_2^* is set as zero point), in which

reaction (8) is rate-determining in the whole process. We also consider CH₃OH production in the final step. By contrast, the free energy for CH₄ production is lower than CH₃OH production, which means CH₄ is more thermodynamically favorable.

In free energy diagram, we can see that $\Delta G(\text{CO}_2 + \text{H}^+ + \text{e}^- \rightarrow \text{COOH}^*)$ and $\Delta G(\text{CO}^* + \text{H}^+ + \text{e}^- \rightarrow \text{CHO}^*)$ are rate-determining steps of CO₂RR. The larger one of them decides onset potential φ , ie, $\varphi = -\max(\Delta G(\text{CO}_2 + \text{H}^+ + \text{e}^- \rightarrow \text{COOH}^*), \Delta G(\text{CO}^* + \text{H}^+ + \text{e}^- \rightarrow \text{CHO}^*))/e$ (see the inset of Figure 1D). By the resulting $\Delta G(\text{CO}_2 + \text{H}^+ + \text{e}^- \rightarrow \text{COOH}^*)$ and $\Delta G(\text{CO}^* + \text{H}^+ + \text{e}^- \rightarrow \text{CHO}^*)$, we determine onset potential of CO₂RR on Ag, Au, Cu, Ni, Pd, Pt, and Rh (111) surfaces with/without graphene overlayer (Figure 1D). The calculated data (Table 3) indicate that graphene overlayer reduces onset potential of CO₂RR by 4% to 19%. The largest decreases of onset potential are found in Ni and Cu (111) surfaces. On bare Cu (111) surface, an onset potential of -1.08 V is needed for CO₂RR. By contrast, on graphene-covered Cu (111) surface, the onset potential is reduced to -0.93 V (Figure 1C). In the free energy diagram, it can be seen that $G(\text{HCOOH})$ is higher than $G(\text{CO}^*)$, which means hydrocarbon production via CO* is more thermodynamically favorable than HCOOH production. In addition, CO molecule may escape from metal surface into gas phase. But CO* → CO(g) is not a redox reaction with electron participation. By the free energy suppression eU of negative electrode potential U , the free energy landscape of the whole CO₂RR process can be much lower than the free energy of CO(g) production, and then CO₂RR to hydrocarbons becomes the main reaction.

3.2 | The effect of graphene on COOH* and CHO*

In the confined space between graphene overlayer and metal surface, the decrease of $\Delta G(\text{CO}_2 + \text{H}^+ + \text{e}^- \rightarrow \text{COOH}^*)$ and $\Delta G(\text{CO}^* + \text{H}^+ + \text{e}^- \rightarrow \text{CHO}^*)$ originates

TABLE 3 Onset potential of CO₂RR with/without graphene

Substrate	Onset Potential/V	
	without Graphene	with Graphene
Ag	-1.25	-1.20
Au	-0.77	-0.71
Cu	-1.08	-0.93
Ni	-1.13	-0.91
Pd	-1.08	-0.97
Pt	-0.67	-0.64
Rh	-0.76	-0.66

from the coupling of graphene to these intermediate molecules (Figure 2A). In confined spaces, the perturbation from microenvironment always enhances system energies. However, graphene overlayer exhibits an effect that leads to smaller free energy increase or even free energy decrease of COOH* and CHO*. To reveal such effect, electron density redistribution between graphene and COOH*/CHO* is displayed in Figure 2B/C, respectively. Calculation results reveal that electrons in the π orbitals of graphene partially transfer to COOH* and CHO*. Redistributed electrons mainly come from the C hexagonal ring of graphene near COOH* or CHO*. To uncover the mechanism, we focus on the coupling between molecular orbitals and metal 3d bands. For detailed theoretical analysis on the orbitals of COOH*, see Appendix S2. The orbitals of σ bonds in COOH* lie in low energy far away from metal 3d bands. Nonbonding $n_{\text{O}2p}^g$ and $n_{\text{O}2p}^u$ orbitals of lone-pair electrons on O atoms and $\pi_{\text{C}2p-\text{O}2p}^g$ and $\pi_{\text{O}2p}^u$ orbitals lie in higher energy (Figure B1(b) in Appendix S2). With energies close to the bottom of metal 3d bands, $n_{\text{O}2p}^g$ and $\pi_{\text{O}2p}^u$ strongly couple with metal 3d bands, resulting in molecular orbital states extending into bands. As an example, projected density of states (PDOS) of Ni-COOH* system and graphene are plotted in Figure 2D, in which the Fermi levels are shown by dashed lines and the PDOS of n_{2p} and π_{2p} is shown by red and blue, respectively. By coupling with Ni 3d bands, the PDOS of n_{2p} and π_{2p} is extended into peaks locating around the Fermi level (for the wavefunctions of original and extended $n_{\text{O}2p}^g$ states, see Figure B2(c) in Appendix S2). With higher Fermi level than Ni-COOH* system, graphene overlayer injects its π_{2p} electrons into the extended molecular $n_{\text{O}2p}^g$ orbitals of COOH*. These injected electrons transfer from high-energy states to low-energy states, resulting in a tendency to resist the repulsion between graphene and molecules.

The same mechanism is also suitable for Ni-CHO*. For detailed theoretical analysis on CHO* molecular orbitals, see Appendix S2. $n_{\text{O}2p}$ and $\pi_{\text{C}2p-\text{O}2p}$ orbitals of CHO* lie in metal 3d bands, resulting in strong coupling and molecular state extension. In Figure 2D, it can be seen that $n_{\text{O}2p}$ and $\pi_{\text{C}2p-\text{O}2p}$ states in Ni-CHO* extend into PDOS peaks around the Fermi level (for the wavefunctions of original and extended $n_{\text{O}2p}$ states, see Figure B3(c) in Appendix S2). With graphene overlayer, electrons inject into the extended molecular orbitals of CHO* and the reaction free energy is then decreased.

In addition, the effect of graphene on the side reaction intermediate HCOO* is weaker than on COOH* and CHO*. On bare metal (111) surfaces, $\Delta G(\text{CO}_2 + \text{H}^+ + \text{e}^- \rightarrow \text{HCOO}^*)$ is in the range of -0.09 to 1.03 eV

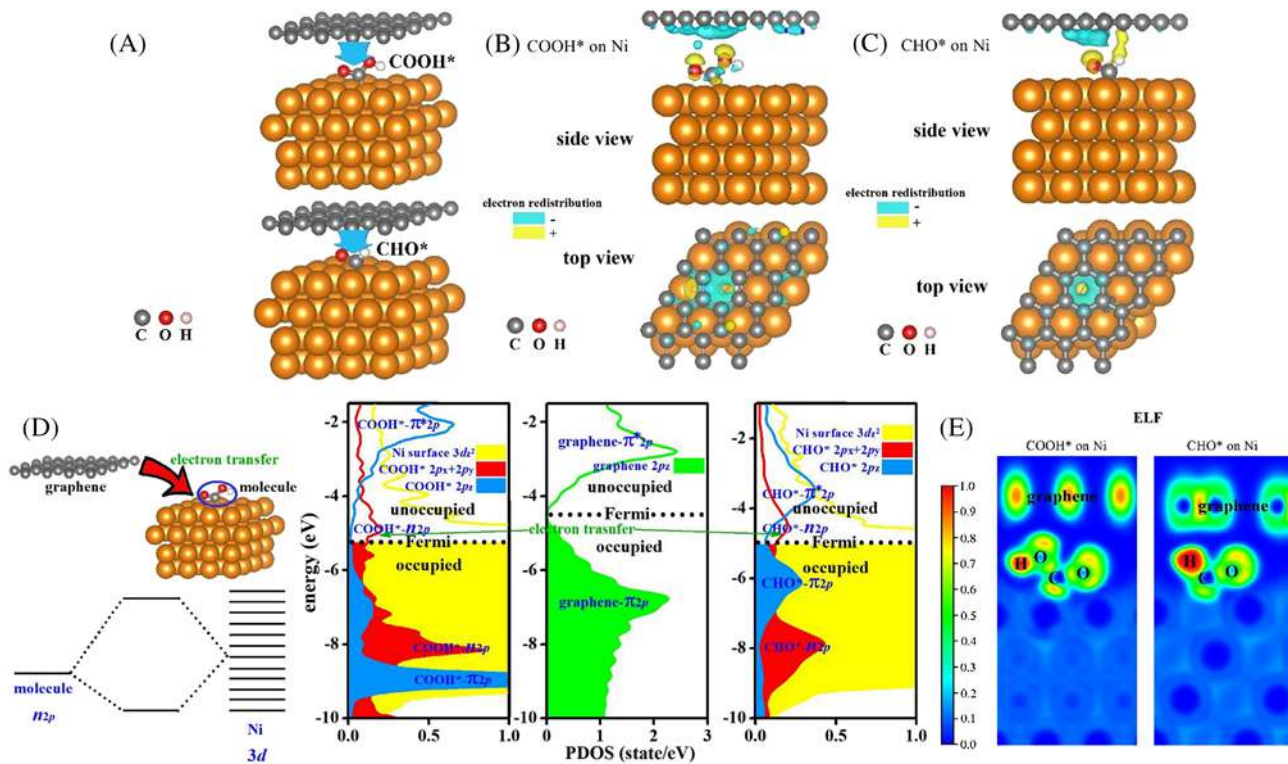


FIGURE 2 The interaction between graphene overlayer and COOH*/CHO*. A, The effect of graphene on COOH* and CHO*. B/C, Electron density redistribution in between graphene and Ni(111)-COOH*/Ni(111)-CHO* system. Isosurfaces of electron redistribution are plotted with values of $\pm 0.001 \text{ e}/\text{\AA}^3$ (yellow/cyan respectively). D, Orbital coupling and projected density of states (PDOS) of bare Ni(111)-COOH* system, isolate graphene and bare Ni(111)-CHO* system. Occupied states are shown by fill areas. The Fermi levels are shown by dashed lines. E, Electron localization function (ELF) in Ni(111)-graphene-COOH* and Ni(111)-graphene-CHO* systems [Colour figure can be viewed at wileyonlinelibrary.com]

(Table A1 in Appendix S1), while on graphene-covered metal (111) surfaces, $\Delta G (\text{CO}_2 + \text{H}^+ + \text{e}^- \rightarrow \text{HCOO}^*)$ is in the range of -0.13 to 1.01 eV (Table A2 in Appendix S1). The decrease in $\Delta G (\text{CO}_2 + \text{H}^+ + \text{e}^- \rightarrow \text{HCOO}^*)$ caused by graphene overlayer is much smaller than the decrease in $\Delta G (\text{CO}_2 + \text{H}^+ + \text{e}^- \rightarrow \text{COOH}^*)$ and $\Delta G (\text{CO}^* + \text{H}^+ + \text{e}^- \rightarrow \text{CHO}^*)$. Graphene overlayer favors to lower the free energies of COOH* and CHO*. Such tendency benefits CO₂RR to hydrocarbons via COOH* and CHO*, and the side reaction via HCOO* is depressed.

To analyze the bonding type between graphene and COOH*/CHO*, electron localization functions (ELFs) of metal-COOH*-graphene and metal-CHO*-graphene are plotted in Figure 2E. It can be seen that electrons are localized in graphene and COOH*/CHO*. The transferred electrons do not form delocalized states between graphene and COOH*/CHO*. Graphene, which partially loses electrons, is positively charged. On the contrary, COOH*/CHO* that gains electrons is negatively charged. So the interaction between graphene and COOH*/CHO* is mainly electrostatic attraction. Since COOH* and CHO* are polar molecules, the gained electrons concentrate on O and H atoms.

3.3 | The scaling law of stabilization energy

To study graphene-molecule interaction strength, the stabilization energy of graphene to molecule is scaled with charge transfer. For COOH*, the stabilization energy on a metal surface is defined as

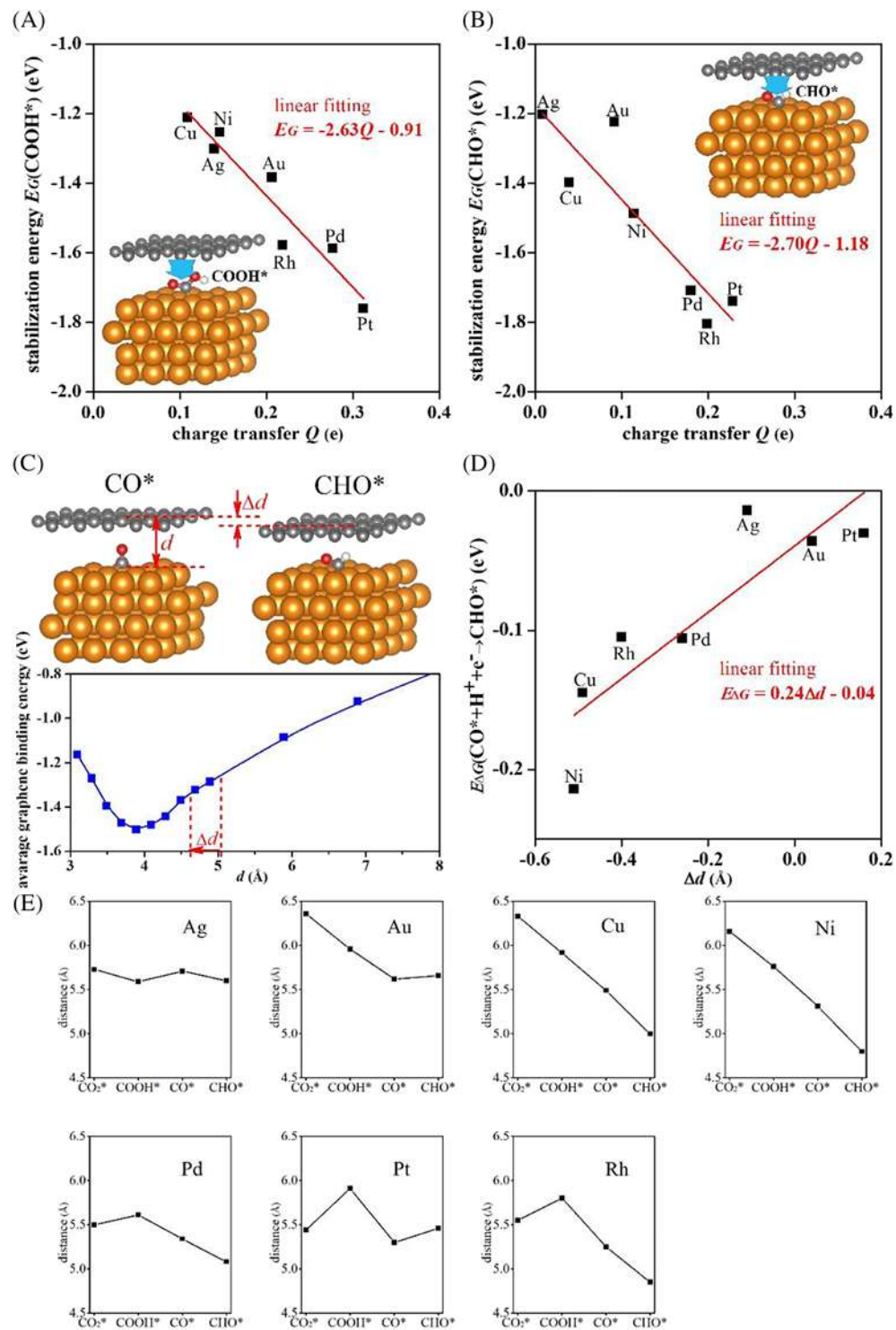
$$E_G(\text{COOH}^*) = G(\text{COOH}^*)_{\text{with graphene}} - G(\text{COOH}^*)_{\text{without graphene}} - G(\text{graphene}) \quad (12)$$

Accordingly, the stabilization energy to CHO* reads

$$E_G(\text{CHO}^*) = G(\text{CHO}^*)_{\text{with graphene}} - G(\text{CHO}^*)_{\text{without graphene}} - G(\text{graphene}) \quad (13)$$

To scale graphene-molecule interaction strength, $E_G(\text{COOH}^*)/E_G(\text{CHO}^*)$ are plotted with electron transfer Q from graphene to COOH/CHO* (Figure 3A/B),

FIGURE 3 Scale the interaction between graphene and adsorbed intermediate molecule. A/B, The stabilization energy $E_G(\text{COOH}^*)/E_G(\text{CHO}^*)$ of graphene to $\text{COOH}^*/\text{CHO}^*$, respectively. C, Upper: the distance d of graphene to metal surface. Lower: average graphene binding energy with d . D, The decrease in $\Delta G(\text{CO}^* + \text{H}^+ + \text{e}^- \rightarrow \text{CHO}^*)$ caused by graphene overlayer, and the distance difference Δd between metal-CO-graphene and metal-CHO-graphene system. E, The distance d of graphene to metal surface during CO_2RR process [Colour figure can be viewed at wileyonlinelibrary.com]



respectively. According to the data, we can see a rough dependency between $E_G(\text{COOH}^*)/E_G(\text{CHO}^*)$ and charge transfer Q . In Figure 3A,B, linear fitting to the data is shown. With more charge transfer from graphene to $\text{COOH}^*/\text{CHO}^*$, the electrostatic interaction between graphene and $\text{COOH}^*/\text{CHO}^*$ is stronger, and therefore, the metal-molecule-graphene system gains more energy decrease, ie, lower $E_G(\text{COOH}^*)/E_G(\text{CHO}^*)$. The extent of charge transfer may relate to the influence of metal

substrate, which controls the Fermi level of the system. Metal substrate with low Fermi level might lead to strong charge transfer from graphene to molecule.

Furthermore, steric hindrance is also a factor to influence reaction free energy. In metal-CO-graphene system, the distance of graphene to metal surface $d(\text{CO}^*)$ is larger than $d(\text{CHO}^*)$ in metal-CHO-graphene system (Figure 3C) because CO^* molecule stands on metal surface. Since the binding energy of graphene and metal

surface varies with graphene-metal distance d , it leads to additional energy difference between metal-CO-graphene and metal-CHO-graphene system. In the lower panel of Figure 3C, graphene binding energy (average value on Ag, Au, Cu, Ni, Pd, Pt, and Rh (111) surfaces) is plotted with d . The difference $\Delta d = d(\text{CHO}^*) - d(\text{CO}^*)$ is signed in the figure. For the reaction $\text{CO}^* + \text{H}^+ + \text{e}^- \rightarrow \text{CHO}^*$, the decrease $\Delta d < 0$ in graphene-metal distance leads to extra free energy decrease, which is defined as

$$E_{\Delta G} = \Delta G(\text{CO}^* + \text{H}^+ + \text{e}^- \rightarrow \text{CHO}^*)_{\text{with graphene}} - \Delta G(\text{CO}^* + \text{H}^+ + \text{e}^- \rightarrow \text{CHO}^*)_{\text{without graphene}} \quad (14)$$

Figure 3D plots $E_{\Delta G}$ on Ag, Au, Cu, Ni, Pd, Pt, and Rh (111) surfaces with corresponding Δd . With more negative Δd , $E_{\Delta G}$ gets lower and a rough linear relation between Δd and $E_{\Delta G}$ can be seen. This result indicates that spatial factor is also an important feature in confined catalysis. To show a full view in the change of d in CO₂RR, Figure 3E plots d for every graphene-metal system with CO₂*, COOH*, CO*, and CHO*. Cu and Ni show downtrend of d along the direction of reaction, meaning that the geometric factor may be advantageous to CO₂RR on graphene-covered Cu or Ni surfaces. On Au surface, d obviously decreases in the CO₂ → COOH* step, while slightly increases in the CO* → CHO* step. So the geometric factor has a little favor to CO₂RR on graphene-covered Au surface.

4 | CONCLUSION

In this work, 2D confined catalytic CO₂RR is investigated by DFT calculations. On Ag, Au, Cu, Ni, Pd, Pt, and Rh surfaces, graphene overlayer exhibits superiority in facilitating CO₂RR. The interactions between graphene and key intermediates (COOH* and CHO*) result in suppression to the reaction free energies of two main steps (CO₂ + H⁺ + e⁻ → COOH* and CO* + H⁺ + e⁻ → CHO*) and decrease in onset potential. On Cu (111) surfaces, the CO₂RR onset potentials are decreased by 0.15 V. The facilitation effect of graphene overlayer on CO₂RR originates from charge transfer to surface molecules. With higher Fermi level than COOH* and CHO*, graphene injects π_{2p} electrons into molecular nonbonding orbitals, resulting in weakening of molecular bonds and electrostatic interactions to lower the reaction free energies. A linear scaling relation between charge transfer and stabilization energy is found. In the step CO* + H⁺ + e⁻ → CHO*, steric hindrance is also a reason to lower reaction free energies. The results indicate important features to

determine reaction free energies in 2D confined catalysis. Our research would provide guidance to future exploration in 2D confined catalysis.

ACKNOWLEDGEMENTS

The authors are grateful to Prof Hao Tang for helpful discussions and for his help in preparing the manuscript. This work is supported by the National Natural Science Foundation of China (nos. 11847047 and 61504031), the Natural Science Basic Research Plan in Shaanxi Province of China (no. 2018JQ1034), the Fundamental Research Funds for the Central Universities (nos. JB180513 and XJS18038), and Postdoctoral Research Project of Shaanxi Province.

ORCID

Zheng-Zhe Lin  <https://orcid.org/0000-0001-7188-6257>

REFERENCES

- Gao S, Jiao XC, Sun ZT, et al. Ultrathin Co₃O₄ layers realizing optimized CO₂ electroreduction to formate. *Angew Chem Int Ed.* 2016;55(2):698-702.
- Cao Z, Kim D, Hong DC, et al. A molecular surface functionalization approach to tuning nanoparticle electrocatalysts for carbon dioxide reduction. *J Am Chem Soc.* 2016;138(26):8120-8125.
- Chang XX, Wang T, Gong JL. CO₂ photo-reduction: insights into CO₂ activation and reaction on surfaces of photocatalysts. *Energ Environ Sci.* 2016;9(7):2177-2196.
- Jiao XC, Chen ZW, Li XD, et al. Defect-mediated electron-hole separation in one-unit-cell ZnIn₂S₄ layers for boosted solar-driven CO₂ reduction. *J Am Chem Soc.* 2017;139(22):7586-7594.
- Najafabadi AT. CO₂ chemical conversion to useful products: an engineering insight to the latest advances toward sustainability Amin Taheri Najafabadi. *Int J Energy Res.* 2013;37:485-499.
- Lais A, Gondal MA, Dastageer MA, Al-Adel FF. Experimental parameters affecting the photocatalytic reduction performance of CO₂ to methanol: a review. *Int J Energy Res.* 2018;42:2031-2049.
- Khrasheh M, Khazndar A, Al-Ghouti MA. Visible light-driven metal-oxide photocatalytic CO₂ conversion. *Int J Energy Res.* 2015;39:1142-1152.
- Hori Y, Wakebe H, Tsukamoto T, Koga O. Electrocatalytic process of CO selectivity in electrochemical reduction of CO₂ at metal electrodes in aqueous media. *Electrochim Acta.* 1994;39:1833-1839.
- Jitaru M, Lowy DA, Toma M, Toma BC, Oniciu LJ. The electrochemical reduction of carbon dioxide on flat metallic electrodes. *J Appl Electrochem.* 1997;27(8):875-889.
- Kuhl KP, Hatsukade T, Cave ER, Abram DN, Kibsgaard J, Jaramillo TF. Electrocatalytic conversion of carbon dioxide to methane and methanol on transition metal surfaces. *J Am Chem Soc.* 2014;136(40):14107-14113.

11. Frese KW Jr. In: Sullivan BP, Krist K, Guard HE, eds. *Electrochemical and Electrocatalytic Reactions of Carbon Dioxide*. New York: Elsevier; 1993:145-216.
12. Hori Y, Takahashi R, Yoshinami Y, Murata A. Electrochemical reduction of CO at a copper electrode. *J Phys Chem*. 1997;B101: 7075-7081.
13. Gattrell M, Gupta N, Co A. A review of the aqueous electrochemical reduction of CO₂ to hydrocarbons at copper. *J Electroanal Chem*. 2006;594(1):1-19.
14. Peterson AA, Abild-Pedersen F, Studt F, Rossmeisl J, Nørskov JK. How copper catalyzes the electroreduction of carbon dioxide into hydrocarbon fuels. *Energ Environ Sci*. 2010; 3(9):1311-1315.
15. Durand WJ, Peterson AA, Studt F, Abild-Pedersen F, Nørskov JK. Structure effects on the energetics of the electrochemical reduction of CO₂ by copper surfaces. *Surf Sci*. 2011; 605(15-16):1354-1359.
16. Hori Y. *Modern Aspects of Electrochemistry*. 42 New York: Springer; 2008:89-189.
17. Chen Z, Ma L, Li S, et al. Simple approach to carboxyl-rich materials through low-temperature heat treatment of hydrothermal carbon in air. *Appl Surf Sci*. 2011;257:8686-8691.
18. Deng D, Novoselov KS, Fu Q, Zheng N, Tian Z, Bao X. Catalysis with two-dimensional materials and their heterostructures. *Nat Nanotechnol*. 2016;11:218-230.
19. Li Y, Xu L, Liu H, Li Y. Graphdiyne and graphyne: from theoretical predictions to practical construction. *Chem Soc Rev*. 2014;43:2572-2586.
20. Weng Q, Wang X, Wang X, Bando Y, Golberg D. Functionalized hexagonal boron nitride nanomaterials: emerging properties and applications. *Chem Soc Rev*. 2016;45:3989-4012.
21. Yan L, Zheng YB, Zhao F, et al. Chemistry and physics of a single atomic layer: strategies and challenges for functionalization of graphene and graphene-based materials. *Chem Soc Rev*. 2012;41:97-114.
22. Hur SH, Park JN. Graphene and its application in fuel cell catalysis: a review. *Asia Pac J Chem Eng*. 2013;8(2):218-233.
23. Novoselov KS, Jiang D, Schedin F, et al. Two-dimensional atomic crystals. *Proc Natl Acad Sci U S A*. 2005;102:10451-10453.
24. Huang C, Li Y, Wang N, et al. Progress in research into 2D graphdiyne-based materials. *Chem Rev*. 2018;118(16):7744-7803.
25. Lv Q, Si W, He J, et al. Selectively nitrogen-doped carbon materials as superior metal-free catalysts for oxygen reduction. *Nat Commun*. 2018;9(1):3376.
26. Lv Q, Si W, Yang Z, et al. Nitrogen-doped porous graphdiyne: a highly efficient metal-free electrocatalyst for oxygen reduction reaction. *ACS Appl Mater Interfaces*. 2017;9(35):29744-29752.
27. Chan K, Tsai C, Hansen HA, Nørskov JK. Molybdenum sulfides and selenides as possible electrocatalysts for CO₂ reduction. *ChemCatChem*. 2014;6:1899-1905.
28. Jiao X, Li X, Jin X, et al. Partially oxidized SnS₂ atomic layers achieving efficient visible-light-driven CO₂ reduction. *J Am Chem Soc*. 2017;139(49):18044-18051.
29. Hu W, Lin L, Zhang R, Yang C, Yang J. Highly efficient photocatalytic water splitting over edge-modified phosphorene nanoribbons. *J Am Chem Soc*. 2017;139(43):15429-15436.
30. An Y-R, Fan X-L, Luo Z-F, Lau W-M. Nanopolymers of monolayer MS₂: best morphology and size for HER catalysis. *Nano Lett*. 2017;17(1):368-376.
31. Yao Y, Fu Q, Zhang YY, et al. Graphene cover-promoted metal-catalyzed reactions. *Proc Natl Acad Sci U S A*. 2014; 111(48):17023-17028.
32. Zhang Y, Weng X, Li H, et al. Hexagonal boron nitride cover on Pt(111): a new route to tune molecule-metal interaction and metal-catalyzed reactions. *Nano Lett*. 2015;15(5):3616-3623.
33. Mu R, Fu Q, Jin L, et al. Visualizing chemical reactions confined under graphene. *Angew Chem-Int Edit*. 2012;51(20):4856-4859.
34. Zhou Y, Chen W, Cui P, et al. Enhancing the hydrogen activation reactivity of nonprecious metal substrates via confined catalysis underneath graphene. *Nano Lett*. 2016;16(10):6058-6063.
35. Fu Q, Bao X. Surface chemistry and catalysis confined under two-dimensional materials. *Chem Soc Rev*. 2017;46:1842-1874.
36. Li H, Xiao J, Fu Q, Bao X. Confined catalysis under two-dimensional materials. *Proc Natl Acad Sci U S A*. 2017;114:5930-5934.
37. Han P, Wang ZJ, Kuang M, et al. 2D assembly of confined space toward enhanced CO₂ electroreduction. *Adv Energy Mater*. 2018;8(25):1801230.
38. Kresse G, Hafner J. Ab initio molecular dynamics for liquid metals. *Phys Rev*. 1993;B47:558-561.
39. Kresse G, Hafner J. Ab initio molecular-dynamics simulation of the liquid-metal-amorphous-semiconductor transition in germanium. *Phys Rev*. 1994;B49:14251-14269.
40. Kresse G, Furthmüller J. Efficient iterative schemes for ab initio total-energy calculations using a plane-wave basis set. *Phys Rev*. 1996;B54:11169-11186.
41. Kresse G, Furthmüller J. Efficiency of ab-initio total energy calculations for metals and semiconductors using a planewave basis set. *Comput Mater Sci*. 1996;6(1):15-50.
42. Blöchl PE. Projector augmented-wave method. *Phys Rev*. 1994; B50:17953-17979.
43. Kresse G, Joubert D. From ultrasoft pseudopotentials to the projector augmented-wave method. *Phys Rev*. 1999;B59:1758-1775.
44. Klimes J, Bowler DR, Michaelides A. Chemical accuracy for the van der Waals density functional. *J Phys Condens Matter*. 2010;22(2):022201.
45. Klimes J, Bowler DR, Michaelides A. Van der Waals density functionals applied to solids. *Phys Rev B*. 2011;83(19):195131.
46. Guo HY, Lu N, Dai J, Wu XJ, Zeng XC. Phosphorene nanoribbons, phosphorus nanotubes, and van der Waals multilayers. *J Phys Chem C*. 2014;118:14051-14059.
47. Padilha JE, Miwa RH, da Silva AJR, Fazzio A. Two-dimensional van der Waals p-n junction of InSe/phosphorene. *Phys Rev B*. 2017;95:6.
48. Cramer CJ. *Essentials of Computational Chemistry: Theories and Models*. 2nd ed. New York: Wiley; 2004.
49. Varley JB, Hansen HA, Ammitzbøll NL, et al. Ni-Fe-S cubanes on CO₂ reduction electrocatalysis: a DFT study. *ACS Catal*. 2013;3(11):2640-2643.
50. Nørskov JK, Rossmeisl J, Logadottir A, Lindqvist L. Origin of the overpotential for oxygen reduction at a fuel-cell cathode. *J Phys Chem B*. 2004;108:17886-17892.

51. Hansen HA, Varley JB, Peterson AA, Nørskov JK. Understanding trends in the electrocatalytic activity of metals and enzymes for CO₂ reduction to CO. *J Phys Chem Lett.* 2013;4(3):388-392.

SUPPORTING INFORMATION

Additional supporting information may be found online in the Supporting Information section at the end of this article.

How to cite this article: Lin Z-Z, Chen X, Yin C, Yue L, Meng F-X. Electrochemical CO₂ reduction in confined space: Enhanced activity of metal catalysts by graphene overlayer. *Int J Energy Res.* 2020;44:784-794. <https://doi.org/10.1002/er.4888>